2006

Condensation and Wetting Behavior on Surfaces With Micro-Structures: Super-Hydrophobic and Super-Hydrophilic

Yongfang Zhong
University of Illinois at Urbana-Champaign at Urbana-Champaign

Anthony M. Jacobi
University of Illinois at Urbana-Champaign at Urbana-Champaign

John G. Georgiadis
University of Illinois at Urbana-Champaign at Urbana-Champaign

Condensation and Wetting Behavior on Surfaces with Micro-Structures: Super-hydrophobic and Super-hydrophilic

Yongfang ZHONG*, Anthony M. JACOBI and John G. GEORGIADIS

Department of Mechanical and Industrial Engineering,
University of Illinois at Urbana-Champaign,
1206 W. Green Street, Urbana, IL, 61801, USA
*Corresponding Author, Phone: 1-217-244-8830, E-mail: yzhong1@uiuc.edu

ABSTRACT

Recently it has become possible to achieve radical manipulation of surface wettability, and wettability is known to play a key role in the retention of condensate and frost melt on heat exchanger surfaces. In this paper we present a review of methods to produce such surfaces, and we describe a super-hydrophobic surface, with a contact angle of 148°, created in our lab. We describe surfaces with micro-posts and micro-grooves, and the wetting behavior of these surfaces and early growth of condensate is studied experimentally. The rapid spreading of droplets is observed for surfaces with silicon grooves and posts while an anisotropic wetting is observed for the droplets on the surface with SU8 grooves. The results of our microscopic observations show that condensate drops group around the posts on the super-hydrophobic surface, but condensate forms a thin film on the surface with silicon posts. Condesnate is drawn into the grooves mainly by surface tension.on the anisotropic surface.

1. INTRODUCTION

When a liquid water droplet rests a solid substrate, a finite angle is formed between the liquid and solid interface at the three-phase contact line. This angle, defined as contact angle (θ), for virtually all real systems lies between 0° and approximately 110°. Complete wetting (θ =0°) or complete non-wetting (θ =180°) is difficult, if not impossible, to achieve on ordinary surfaces. Only recently super-hydrophobic surfaces with contact angles of approximately 150° or greater have been produced in laboratories. A review of methods to produce such surfaces is provided in Table 1, along with a list of the procedures and materials, equilibrium contact angles (θ_e), maximum advancing contact angles ($\theta_{a,max}$), corresponding receding contact angles ($\theta_{r,max}$), and contact angle hysteresis ($\Delta\theta$) manifested by the surface. The procedures to generate such surfaces vary significantly from chemical reactions to classical photolithography techniques. The materials used to produce such surfaces can be metals (copper or aluminum), silicon, polymer (SU-8 photoresist), silicone (PDMS), wax (AKD) and others. Although super-hydrophobic surfaces reported in the open literature span a range of materials and methods, the two basic principles underlie all these approaches for creating super-hydrophobic surfaces: 1) The roughness of these surfaces is very large, and the distance between two adjacent asperities on the surface and the size of the asperity are on the order of micrometers or nanometers. 2) The surface energy of the surface material is low, that is, the contact angle on an ordinary flat surface made of the same material without micro-scale asperities is relatively large. Therefore, not only the chemical properties of the surfaces but also their geometry contribute to achieving super-hydrophobicity.

Significant attention has been directed at how to make such surfaces, the motion of droplets on the surfaces, and the mechanisms causing high hydrophobicity. Quere and Bico *et al.* (1999) condensed water vapor to study contact angle hysteresis and sliding angle on a super-hydrophobic surface. The contact angle was 164° and contact angle hysteresis was 5° when a droplet was deposited on the surface. When a drop was formed by condensation, the contact angle was 141° and the hysteresis is 100 to105°. No explanation was provided. To our knowledge, this is the only paper available in the open literature reporting condensation on super-hydrophobic surfaces. In work now reported, wetting behavior and microscopic observations of condensation are described for a super-hydrophobic surface and surfaces with micro-structures.

Table 1. A review of the procedure to produce super-hydrophobic surfaces

procedure	θ_e (°)	$\theta_{a,max}$ (°)	$\theta_{r,max}$ (°)	$\Delta\theta$ (°)	references
oxygen plasma treated PTFE	--	171	162	9	Morra(1989), Coulson (2000)
polymerization combined with hydrophobic silicium dioxide	156	--	--	--	Murase (1994)
vacuum-deposited PTFE powder on glass plates	--	146	60	86	Miller (1996)
solidification of AKD (a kind of wax) to form a fractal surface	174	--	--	--	Shibuichi (1996), Onda (1996)
porous Al_2O_3 film, coated by a water-repellent agent(FAS), on glass plates	165	168	150	18	Tadanaga (1997), Shibuichi (1998)
FAS or TMS film by PECVD	160	--	--	--	Hozumi (1997, 1998)
phase separation of organic paint with SiO_2 particles	>150	--	--	--	Sasaki, (1998)
micro-structured silicon surfaces coated by fluorosilane	--	170	155	15	Bico, (1999)
silica or boehmite films coated by fluoroalkylsilane	152	--	--	--	Nakajima(1999, 2000)
plasma polymerization; plasma etching; surfaces with compressed PTFE particles	--	172 ~ 177	169 ~177	0 ~3	Chen (1999), Youngblood (1999)
silane-coated silicon surfaces with posts in different shapes	--	176	156	20	Oner (2000)
plasma-polymerized fluorocarbon film using CH_4/C_4F_8 gas	>150	--	--	--	Matsumoto (2000)
boehmite film surface coated with FAS-17	160	--	--	---	Miwa (2000)
polymer nanofibers and carbon nanotubes	166	--	--	--	Feng (2002)
DRIE etching on silicon and then coat with Teflon	>175	--	--	--	Joonwon (2002)
micro-structured silicon surface coated with fluoroalkylsilane	155	--	--	--	Yoshimitsu (2002)
sol-gel phase-separation process	--	156	152	4	Shirtcliffe (2003)
carbon nanotubes with PTFE coating	--	170	160	10	Lau (2003)
tin (Sn) film on silicon wafer	~ 85	~ 152	~139	~ 13	Uelzen (2003)
micro-structured PDMS surfaces	152	--	--	--	He (2003)
micro-posts made of SU-8 treated with fluorocarbon	147	154	100	54	Shirtcliffe (2004), McHale (2004)
copper surfaces with pillar structures from electrodeposition, and then coated with fluorocarbon	160	--	--	--	Shirtcliffe (2004)
nano-structured polymeric surfaces, aluminum sheet or aluminum oxide	--	156	148	8	Lee (2004)
porous gold film formed by electrodeposition	131	--	--	--	Eabdelsalam (2005)
silicon with micro-structures and commercially Al, copper, gold foils which coated with a fluorinated agent	165	--	--	--	Furstner (2005)
copper from etching or eletrodeposition and then coated with fluorocarbons	155	--	---	--	Shirtcliffe (2005)

2. EXPERIMENTAL APPARATUS

The experimental apparatus shown in Figure 2, consisting of an aluminum open-loop wind-tunnel, TS-4ER thermal microscope stage, a scanning confocal microscope (SCM) and a data acquisition and control system has been developed to conduct experiments on the inception of condensation and frost formation with chemically and physically modified super-hydrophobic surfaces. The wind-tunnel controls the conditions of the air flowing over test substrates, and temperature and humidity are set to mimic air-conditioning and refrigeration conditions. The TS-4ER thermal microscope stage cools test substrates to a setting temperature. The scanning confocal microscope is used to observe the frost growth at the scale of microns.

The wind tunnel flow channel provide a controlled air flow over the test substrates and is placed on the stage of the SCM under its objectives. The air channel is a 500 mm long section with a rectangular cross-section 3 mm high, 8 mm wide, with an inlet contraction of 5.25:1. Three screens are installed in the contraction to help provide a uniform velocity profile. The test section for substrates is located 30 mm downstream from the contraction and 300mm (more than 25 hydraulic diameters in length) downstream from the entrance of airflow. A glass window is installed above the test section to provide optical access for visualization during condensation or frost growth. Type E thermocouples are installed to measure the air temperatures upstream

and downstream of the test section. The air temperature is set by passing the air flow through conditioning passages, through which an ethylene-glycol-water mixture circulates. The temperature of ethylene-glycol-water mixture is controlled by a thermal bath and pumped to the wind tunnel. The airflow in the wind tunnel is supplied from a compressed air tank. Before entering the wind tunnel, the airflow is divided into three streams and two of them bubble through water, so that the humidity of the airflow can be controlled by adjusting the ratio of these streams. A 2-liter plenum with a capacitance-film sensor is placed in the airflow before it enters the wind tunnel to measure the humidity. After the air flows into the wind tunnel, its temperature is set by adjusting the conditions of the ethylene-glycol flow and letting the air, the wind channel and the ethylene-glycol flow reach steady state. The airflow exits the wind tunnel and enters the laboratory. Rotometers are used to measure the volumetric flow rate in each stream. During experiments, the wind tunnel is well insulated to isolate it from the ambient, and a flow of nitrogen is used to blow away the ambient air above the glass window, in order to avoid condensation on the viewing window of the SCM.

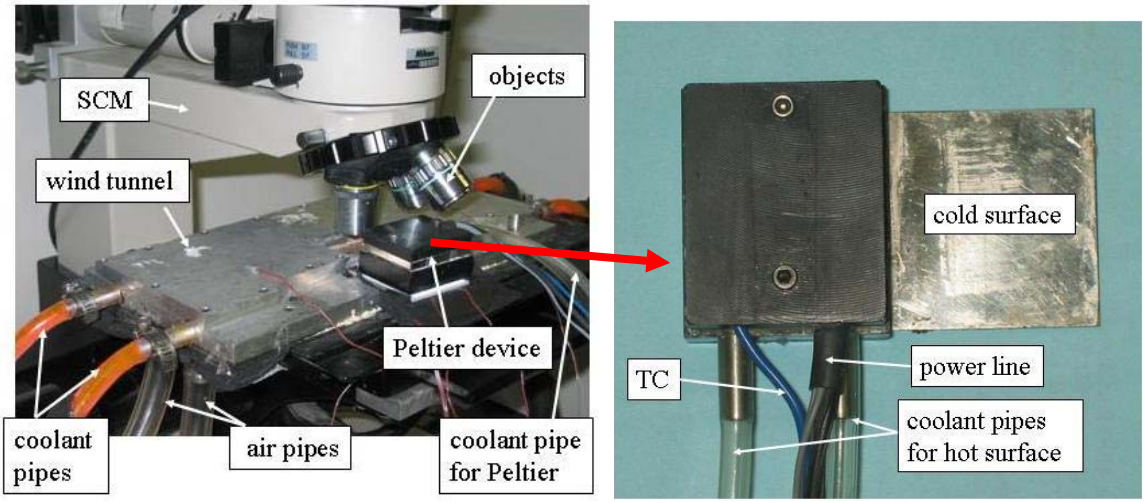

Figure 1 (a)wind-tunnel with the test section under the objectives of SCM; (b) thermoelectric (Peltier) device with a thermocouple (TC) to control the temperature of cold surface.

A PC-based data acquisition system (National Instruments) is used to collect the real-time experimental data and to control the motion of the SCM. The uncertainties of the measured variables are as follows: ±0.2 °C for the air temperatures in the wind tunnel; ±0.1°C for the temperature of the Peltier cold surface; ±0.1°C for the air temperature measured by humidity transmitter; ±1% for the relative humidity in the range from 0 to 90% and ±2% between 90% and 100%; ±0.1 μm for the vertical position of the SCM stage; and ±0.5 liter/min for the airflow rate. The experimental apparatus was tested to check the repeatability and stability of the measured parameters. Over the course of an experiment, the maximum temperature variation of the copper surface attached to the cold Peltier was ±0.31°C over an 8 cm^2 area exposed to room-temperature quiescent air; the variation of humidity ratio of the airflow was ±0.00016 kg-water/kg-dry-air over a period of one hour and thirty minutes; the temperatures of the airflow in the wind tunnel had a variation of± 0.05 °C over a period of two hours and twenty six minutes. Prior to an experiment, a stream of dry nitrogen flows through the wind tunnel. Inside the wind tunnel, the temperature of the nitrogen flow and the test substrate are set to the desired temperature. Outside the wind tunnel, the airflow is to the desired humidity ratio. An experiment is initiated by switching the dry nitrogen flow to airflow.

In these experiments, silicon wafers were used to make substrates with various surface morphologies. Clearly, in air-dehumidification systems the heat exchanger will not be made from silicon. The use of silicon allows for a highly controlled surface, both in terms of geometric shape and dimension, and in terms of chemistry. The processing and control of micro-scale structures and surface chemistry are well established for silicon; therefore, it allows for study of structure and chemistry effects in a controlled way. Ultimately, the phenomena under study here are likely to be exploited with aluminum or other conventional heat exchanger materials. There are good reasons to believe that microstructure can be imparted to aluminum in a roll-to-roll

process, at a low cost. We used standard photolithography methods to create patterns on the surface of silicon. The silicon wafers are one-side polished, test grade, (type N, silicon 100), 100 mm in diameter and 475 – 575 μm thick. In order to modify the surface topography, we used a two-step process: (1) we transferred designed patterns to the photoresist layer on the silicon surface, and then (2) we used an Inductively Coupled Plasma–Deep Reactive Ion Etching process to make micro-structures as shown in Figure 2.

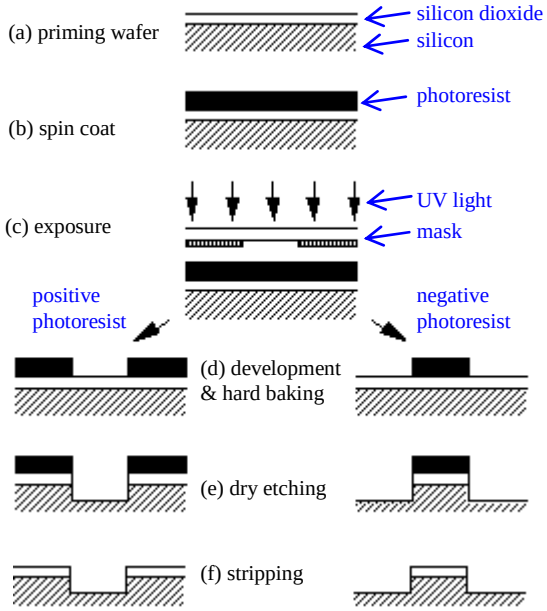

Figure 2 photolithography method used to modify surface topography

3. RESULTS AND DISCUSSION

3.1 Wetting Behavior of Sessile Droplets

The geometric specifications for the sample surfaces are provided in Table 2. The feature sizes of the patterns are given as diameter or width, and height. An image of the contact angle on sample #1 and an image of its surface structure are provided in Figure 3. The contact angle on sample #1 is 148° (for a 3 mm-diameter droplet). The contact angle on smooth, untreated silicon is 42° (for a 1 mm droplet) and the contact angle on a flat polydimethylsiloxane (PDMS) surface is reported to be 114° [Lee *et al.* (2005)] (we measured 113°). Water droplets on samples #2 to #3 quickly wicked into the surface structures and formed a thin film. A Scanning Electron Microscope image of the surface of Sample #2 is shown in Figure 4. The surface structure of Sample #4 consists of grooves as shown in Figure 5, constructed of SU-8. It has been reported that the contact angle on a flat SU-8 surface is 80° [McHale *et al.* (2004)]. Thus, this surface composes of two materials: silica with a contact angle of 40° and SU-8 with a higher contact angle. When droplets are deposited on Sample #4, two values of the contact angle are observed when droplets are viewed from different directions: approximately 128° when viewed parallel to the channel and 65° when viewed perpendicular to the channel. This behavior is different from that on Sample #3 whose surface is a uniform silicon wafer surface and on which water droplets are wicked into the microchannel right after deposition.

Table 2. Characteristics of the sample surfaces

Surface structure	Sample #1	Sample #2	Sample #3	Sample #4
Shape	circular	square	groove	groove
Diameter or width (μm)	20	30	30	30
Height (μm)	21	24	24	26
Distance between rows (μm)	40	30	30	30
Equilibrium contact angle (°)	148	0	0	depends
Droplet sliding angle (°)	< 5	–	–	–
Droplet diameter (mm)	3	–	–	–
Surface material	PDMS	silica	silica	silica + SU-8

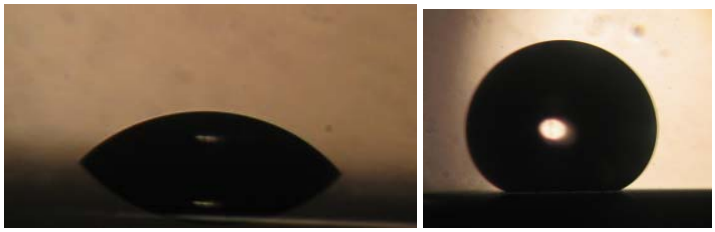

(a) (b)

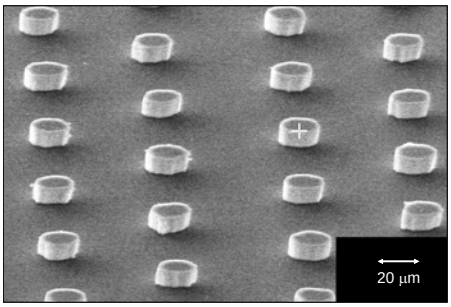

(c)

Figure 3. (a) water droplet (d=1mm) on untreated silicon surface; (b) water droplet (d=3mm)on sample #1; (c) SEM microscopy image of sample #1.

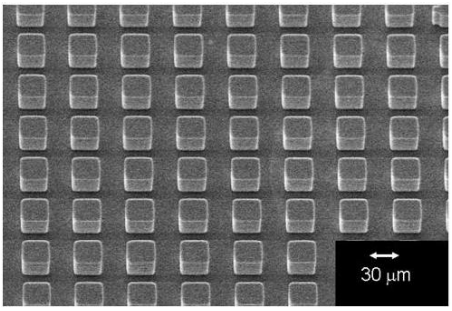

Figure 4 SEM image of Sample #2

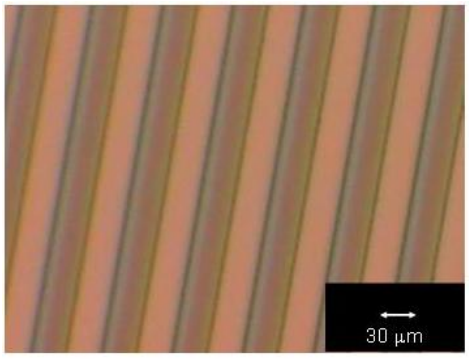

(a)

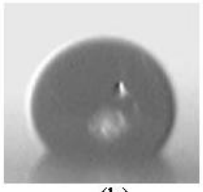

(b)

(c)

Figure 5. Sample #5 made of SU-8 (a) microscopic image; (b) droplet viewed parallel to the microchannel; (c) the same droplet viewed perpendicular to the microchannel.

3.2 Microscopic Observation of Condensation

Preliminary observations demonstrate that the behavior of the contact line on topographically modified surfaces is much more complex than on conventional surfaces. Surface modification generates patterns in the motion of the liquid phase as shown in Figure 6. At the initial stage, when droplets are much smaller than the

surface features, droplets appear everywhere–the top surface of posts and the surface between the posts on both Sample #1 and #2. As the condensate accumulates, the droplets group together around posts on Sample #1, while condensate forms a thin film on Sample #2. This behavior is an important factor influencing condensate retention and frost growth. The density and conductivity of the frost layer growing from dropwise condensate (Sample #1) must vary significantly from that growing from filmwise condensate (Sample #2).

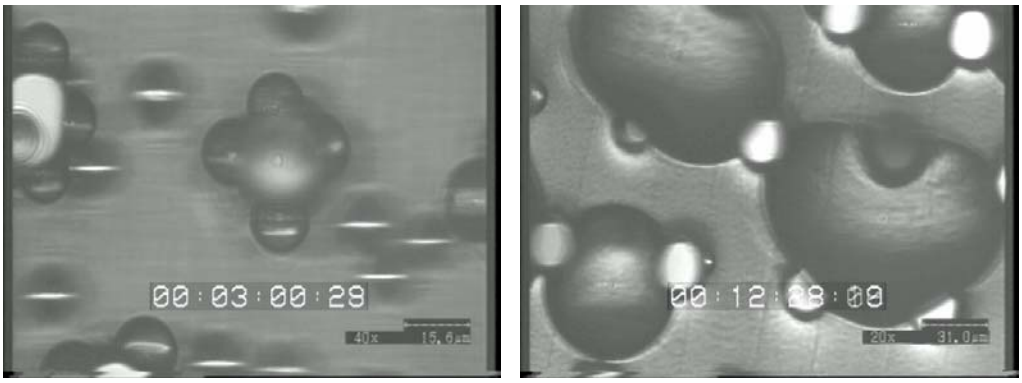

(a) Condensate with Sample#1 @ T_{air} = 21.1°C; RH = 51.7%; substrate @ 1.8 °C

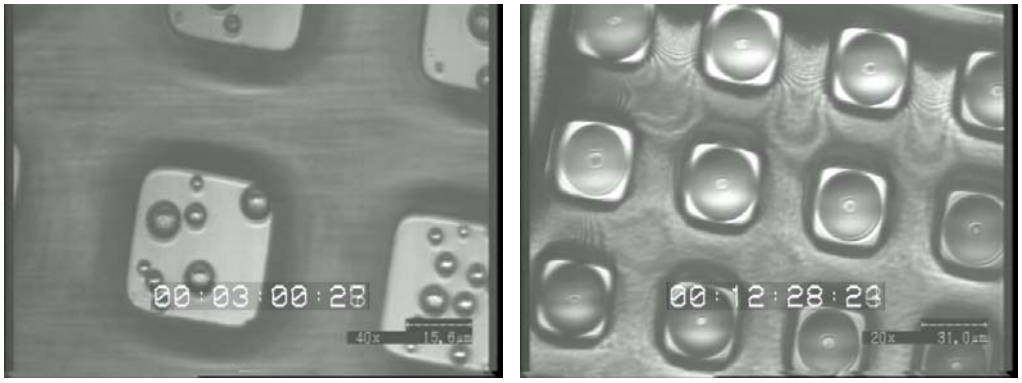

(b) Condensate with Sample #2 @ T_{air} = 20.6°C; RH = 52.7%; substrate @ 1.5°C

Figure 6. Different patterns of condensate on Sample #1 and #2.

Microscopic observations of condensation on Samples #3 and #4 under the similar environmental conditions are shown in Figure 7. On both Sample #3 and #4, condensate appears on both the top surface and bottom surface of the micro-grooves. Once the condensate on the top surface accumulates to certain amount, it falls into the grooves. The condensate on the bottom surface of the grooves is moved by surface tension and drawn to form big droplets which cover several grooves. There are a few differences in condensate between the SU8 grooves and the silicon grooves. The time to grow new condensate on silicon grooves is shorter than that on SU8 grooves after the condensate on the top surface falls into the grooves. Because the amount of condensate observed during the experiments is very small, it is expected that gravity does not play a role in the motion of the condensate. Instead, surface tension may be the dominant force to drive the movement.

4. CONCLUSIONS

Super-hydrophobic surfaces have attracted significant attention recently. In this paper, a review of the methods to produce such surfaces is provided. A super-hydrophobic surface and surfaces with micro-structures are successfully generated, and the wetting behavior and the growth of condensation on these surfaces are studied in the experiments. The preliminary results show:

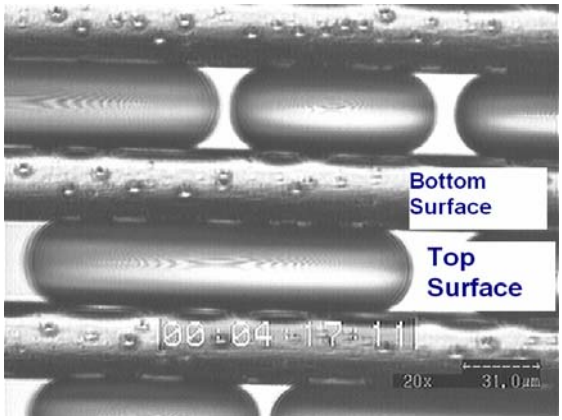

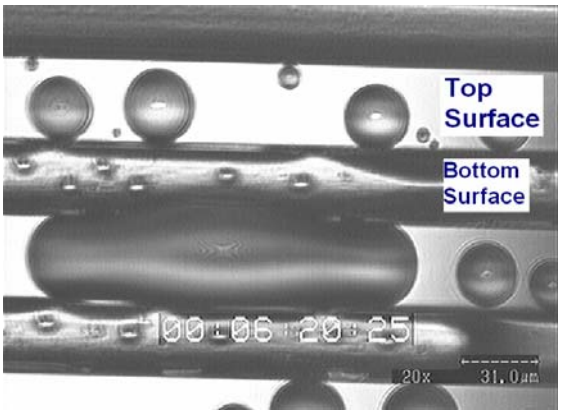

(a) Condensate coalescence on Sample #3 (silicon grooves)

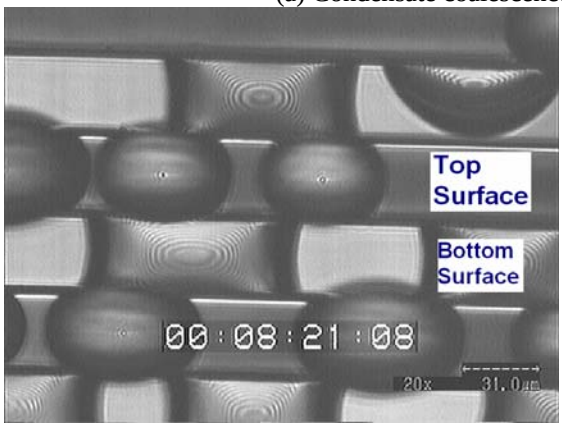

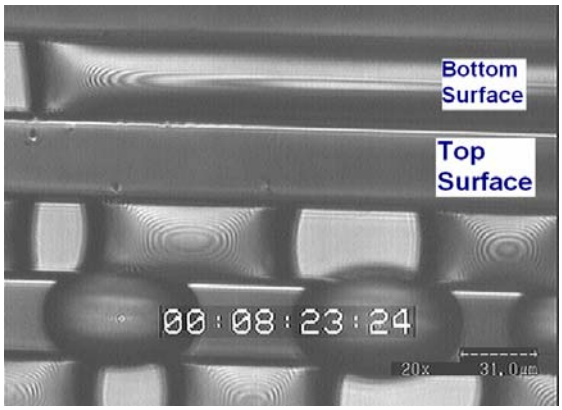

(a) Condensate coalescence on Sample #4 (SU8 grooves)

Figure 7 Microscopic observation of condensation on micro-grooved surfaces

- Sessile droplets form a truncated sphere, with a contact angle of 148° on the super-hydrophobic sample, but spread rapidly to form a thin film on the surfaces with silicon posts and grooves. An anisotropic wetting is found on the surface with SU8 grooves.
- Condensate appears everywhere on the surfaces when it is smaller than the dimension of micro-structures. There are significant difference during the coalescence of droplets on surfaces with different structures.Droplets can group around the posts, form a thin film, or fall into the grooves. This behavoir could play a role on macro-scale condensate drainage and frost formation after.

REFERENCES

Bico, J., C. Marzolin, and D. Quere, 1999.Pearl Drops. *Europhysics Letters*, 47(2): p. 220-226.

Chen, W., et al., 1999. Ultrahydrophobic and ultralyophobic surfaces: Some comments and examples. *Langmuir*, 15(10): p. 3395-3399.

Coulson, S.R., et al., 2000, Super-repellent composite fluoropolymer surfaces. *Journal of Physical Chemistry B*, vol 104, no 37: p. 8836-8840.

E.Abdelsalam, M., et al., 2005.Wetting of Regularly Structured Gold Surfaces. *Langmuir*, 21: p. 1753-1757.

Furstner, R., et al., 2005,Wetting and Self-Cleaning Properties of Artificial Superhydrophobic Surfaces. *Langmuir*,. 21: p. 956-961.

Feng, L., et al., 2002.Super-hydrophobic surfaces: From natural to artificial. *Advanced Materials*, 14(24): p. 1857-1860.

He, B., N.A. Patankar, and J. Lee, 2003.Multiple equilibrium droplet shapes and design criterion for rough hydrophobic surfaces. *Langmuir*, 19(12): p. 4999-5003.

Hozumi, A. and O. Takai, 1997.Preparation of ultra water-repellent films by microwave plasma-enhanced CVD. *Thin Solid Films*, 303(1-2): p. 222-225.

Hozumi, A. and O. Takai, 1998.Preparation of silicon oxide films having a water-repellent layer by multiple-step microwave plasma-enhanced chemical vapor deposition. *Thin Solid Films*, 334(1-2): p. 54-59.

Joonwon Kim and C.-J.C. Kim, 2002. Nanostructured surfaces for dramatic reduction of flow resistance in droplet-based microfluidics. IEEE.

Lau, K.K.S., et al., 2003.Superhydrophobic Carbon Nanotube Forests. *Nano Letters*, 3(12): p. 1701-1705.

Lee, W., et al., 2004, Nanostructuring of a polymeric substrate with well-defined nanometer-scale topography and tailored surface wettability. *Langmuir*,. 20(18): p. 7665-7669.

Lee, J., B. He, and N.A. Patankar, 2005.A roughness-based wettability switching membrane device for hydrophobic surfaces. *Journal of Micromechanics and Microengineering*, 15(3): p. 591-600.

Matsumoto, Y. and M. Ishida, 2000.The property of plasma-polymerized fluorocarbon film in relation to CH4/C4F8 ratio and substrate temperature. *Sensors and Actuators a-Physical*, 83(1-3): p. 179-185.

McHale, G., et al., 2004. Topography Driven Spreading. *Physical Review Letters*, 93(3): p. 036102-1-036102-4.

Miller, J., et al., 1996,Effect of roughness as determined by atomic force microscopy on the wetting properties of PTFE thin films. *Polymer Engineering and Science*, vol 36, no.14: p. 1849-1855.

Miwa, M., et al., 2000.Effects of the surface roughness on sliding angles of water droplets on superhydrophobic surfaces. *Langmuir*, 16(13): p. 5754-5760.

Morra, M., E. Occhiello, and F. Garbassi, 1989, Contact-Angle Hysteresis in Oxygen Plasma Treated Poly(Tetrafluoroethylene). *Langmuir*, vol.5, no.3: p. 872-876.

Murase, H., et al., 1994. Interactions between Heterogeneous Surfaces of Polymers and Water. *Journal of Applied Polymer Science*, vol 54, no 13: p. 2051-2062.

Nakajima, A., et al., 1999. Preparation of transparent superhydrophobic boehmite and silica films by sublimation of aluminum acetylacetonate. *Advanced Materials*, 11(16): p. 1365-1368.

Nakajima, A., et al., 2000.Transparent superhydrophobic thin films with self-cleaning properties. *Langmuir*, 16(17): p. 7044-7047.

Onda, T., et al., 1996,Super-Water-Repellent Fractal Surfaces. *Langmuir*, vol 12, no. 9: p. 2125-2127.

Oner, D. and T. McCarthy, 2000.Ultrahydrophobic surfaces. Effects of topography length scales on wettability. *Langmuir*, 16(20): p. 7777-7782.

Sasaki, H. and M. Shouji, 1998,Control of hydrophobic character of super-water-repellent surface by UV irradiation. *Chemistry Letters*, (4): p. 293-294.

Shirtcliffe, N., et al., 2003. Intrinsically superhydrophobic organosilica sol-gel foams. *Langmuir*, 19(14): p. 5626-5631.

Shirtcliffe, N.J., et al., 2004.The use of high aspect ratio photoresist (SU-8) for super-hydrophobic pattern prototyping. *Journal of Micromechanics and Microengineering*, 14: p. 1384–1389.

Shibuichi, S., et al., 1996, Super water-repellent surfaces resulting from fractal structure, *J. of Physical Chemstry*, vol 100, no.50: p. 19512-19517.

Shirtcliffe, N.J., et al., 2005.Wetting and Wetting Transitions on Copper-Based Super-Hydrophobic Surfaces. *Langmuir*, 21: p. 937-943.

Shibuichi, S., et al., 1998. Super water- and oil-repellent surfaces resulting from fractal structure. *Journal of Colloid and Interface Science*, vol 208, no. 1: p. 287-294.

Tadanaga, K., N. Katata, and T. Minami, 1997, Super-water-repellent Al2O3 coating films with high transparency, *Journal of the American Ceramic Society*, vol 80, no. 4: p. 1040-1042.

Tadanaga, K., N. Katata, and T. Minami, 1997.Formation process of super-water-repellent Al2O3 coating films with high transparency by the sol-gel method. *Journal of the American Ceramic Society*, vol 80, no. 12: p. 3213-3216.

Uelzen, T. and J. Muller, 2003.Wettability enhancement by rough surfaces generated by thin film technology. *Thin solid films*, 434: p. 311-315.

Youngblood, J.P. and T.J. McCarthy, 1999,Ultrahydrophobic polymer surfaces prepared by simultaneous ablation of polypropylene and sputtering of poly(tetrafluoroethylene) using radio frequency plasma. *Macromolecules*. 32(20): p. 6800-6806.

Yoshimitsu, Z., et al., 2002.Effects of Surface Structure on the Hydrophobicity and Sliding Behavior of Water Droplets. *Langmuir*, 18: p. 5818-5822.

ACKNOWLEDGEMENT

This work was financially supported by the Air-Conditioning and Refrigeration Center, an NSF-founded Industry-University Cooperative Research Center. Their support is gratefully acknowledged.